The 9th European Congress on Computational Methods in Applied Sciences and Engineering
ECCOMAS Congress 2024
3–7 June 2024, Lisboa, Portugal

ADJOINT BASED AERODYNAMIC SHAPE OPTIMIZATION OF A MISSILE ENGINE INLET COVER

ARDA OZUZUN[1] AND ISMAIL H. TUNCER[2]

Aerospace Engineering Department
Middle East Technical University
06800 Ankara, Turkey
[1] e-mail: arda.ozuzun@metu.edu.tr
[2] email: ismail.h.tuncer@ae.metu.edu.tr

Key words: Computational Fluid Dynamics, Aerodynamic Shape Optimization, Discrete Adjoint, Free Form Deformation Box, SU2

Summary. This study addresses the aerodynamic shape optimization of a missile engine inlet cover, a component designed to prevent windmilling on the gas turbine engines during the gliding phase of the missiles. The adjoint-based optimization is conducted with the open-source SU2 software suite. The inlet cover is placed into a Free Form Deformation box and the lattice points of the box become the design variables. The design objectives are to minimize the drag and to maximize the opening moment of the inlet cover at the same time. Both single and multi-objective optimizations with weight factors are performed. The findings are discussed in detail, and it is shown that the optimization process provides novel cover shapes for increased aerodynamic performance compared to the quarter-spherical baseline cover.

1 INTRODUCTION

UCAVs and jet fighters are commonly equipped with guided missiles. Air-breathing cruise missiles are one of them and hold significant importance in military missions. As a propulsion system, gas turbine engines are preferred for cruise missiles. One of the most critical factors in the design of a cruise missile is maximizing its operational range. Therefore, the aerodynamics of the missile play a vital role in achieving low-drag missile configuration. Any protuberance or component on the missile that generates extra drag may significantly reduce its range. As a result, every component mounted on the missile, whether it remains attached for the entire mission or is used during just a part of the mission, must be aerodynamically optimized to maximize the range.

An inlet cover is a component that remains attached to the missile during a specific phase of the mission. Once the aircraft launches the missile the missile engine cannot be started instantly since specific flight conditions must be met for the ignition. Therefore, the missile glides until it reaches a certain speed. The inlet cover is designed to prevent windmilling on the engine during the gliding phase, and it is jettisoned before the engine ignition [1]. Pictures of the inlet cover are given in Figure 1. Optimizing the aerodynamic shape of the cover is crucial to minimize the drag of the gliding configuration and increase the gliding range. Also, it is desired that the cover have a moment in the opening direction around the hinge axis for safe separation. Figure 2 depicts an illustration of the missile launch from an aircraft and the subsequent removal of

Figure 1: SOM Cruise Missile

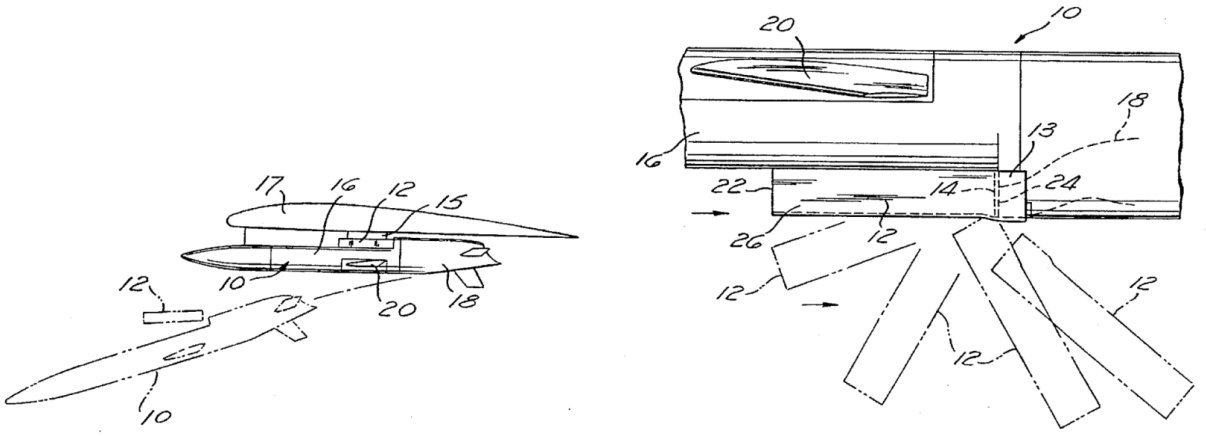

Figure 2: Illustration of Inlet Cover [3]

the inlet cover. The cover is represented by the 12^{th} component in the figure. In this study, aerodynamic shape optimization of the inlet cover is carried out using a generic cruise missile configuration. Gradient-based optimization is performed using the discrete adjoint method since it offers benefits for optimization problems that have a high number of design variables [2].

2 METHOD

In this work, the open-source SU2 software suit is employed to solve Reynolds-Averaged Navier-Stokes equations with the finite volume method and the discrete adjoint equations to obtain objective sensitivities. The flow domain is discretized with unstructured tetrahedral grids. The inlet cover is placed into a Free Form Deformation (FFD) box. The optimization tool, FADO [4], drives the gradient-based optimization process with constrained optimization variables.

2.1 Turbulent Flow Solutions with SU2

In the SU2 flow solver, several key settings are employed to ensure the accurate and efficient computation of turbulent flow solutions. The Jameson-Schmidt-Turkel scheme is used for the convective flux scheme. Time discretization is achieved through the Euler Implicit method,

which allows for larger time steps and improved computational efficiency. For solving large, sparse linear systems, the Flexible Generalized Minimal Residual method is selected as the linear solver. The Green-Gauss method is employed for the gradient reconstruction of the flow variables. Additionally, the Venkatakrishnan flux limiter is applied to the flow and turbulence equations to prevent unphysical oscillations.

2.2 Discrete Adjoint Solver

The sensitivity derivatives of the objective function with respect to the optimization variables are evaluated by the discrete adjoint solver of the SU2 solver suite. It is obtained by the automatic differentiation of the source code of the flow solver in reverse mode. The adjoint solver takes the flow solution as input and evaluates the total derivative of the objective function by solving the system of equations in the differentiated code. The adjoint method is highly efficient for large-scale optimization problems since the computational cost remains independent of the number of design variables.

2.3 Free Form Deformation Box

The Free Form Deformation box serves as an efficient tool to represent boundary surfaces for aerodynamic shape optimization. It offers a CAD-independent parametrization directly applicable to computational grids. Utilizing Bezier curves for deformation, the FFD box employs Bernstein polynomials based on the number of lattice points. The lattice points over the box allow localized changes that collectively shape the whole design surface. The parametrization equation for FFD is:

$$X(u,v,w) = \sum_{i=0}^{l}\sum_{j=0}^{m}\sum_{k=0}^{n} P_{i,j,k} B_i^l(u) B_j^m(v) B_k^n(w) \tag{1}$$

where l, m, and n represent the number of lattice points along each direction within the three-dimensional space, and u, v, w are parameters of Bernstein polynomials ranging between 0 and 1. $P_{i,j,k}$ represents the coordinates of the lattice point indexed by i, j, and k, while $B_i^l(u)$, $B_j^m(v)$, and $B_k^n(w)$ denote Bernstein polynomials. This parameterization equation facilitates smooth deformation, enhancing optimization by reducing design variables while preserving control and flexibility.

2.4 FADO: Framework for Aerostructural Design Optimization

The SU2 software suit has a built-in shape optimization framework for conducting various optimization tasks. However, it is not utilized in this work due to special requirements within the optimization problem, such as the need to bound each design variable separately and employ distinct controls for flow and adjoint solvers. Instead, the Framework for Aerostructural Design Optimization (FADO) is utilized [4]. FADO uses text files for inputs and outputs. It drives the solvers to make the optimization workflow easy. This study employs the SLSQP (Sequential Least Squares Quadratic Programming) optimization algorithm from the SciPy library. The optimization algorithm is widely used and exhibits considerable performance advantages in aerodynamic shape optimization problems [5]. The diagram in Figure 3 illustrates the iterative optimization process.

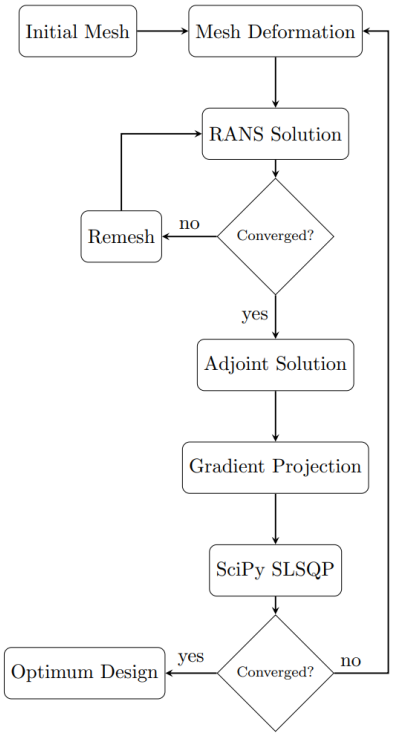

Figure 3: FADO Driven Optimization Process

3 RESULTS AND DISCUSSION

A baseline configuration inspired by an anti-ship cruise missile is selected for optimization studies. The design condition is similarly selected by considering real-world operational scenarios. The sufficient number of lattice points in the FFD box is determined prior to the optimization studies. Three optimization cases are considered. Firstly, a single objective drag minimization of the inlet cover is studied. Secondly, a single objective opening moment maximization of the inlet cover with the drag constraint is targeted. Finally, multi-objective optimizations with weighted objectives are performed.

3.1 Baseline Configuration and Design Condition

The baseline configuration includes a cylindrical fuselage with a spherical nose and an engine inlet cover. The diameter of the missile, measuring 0.3 meters is taken as the reference length. Similarly, the reference area is defined as the cross-sectional area of the fuselage. The baseline configuration and its dimensions are illustrated in Figure 4. There are four components that constitute the inlet assembly. Each of them is presented in a distinct color. In this study, the inlet cover is the design surface. Then, there is a component lip that has the capture area and takes the flow to the internal duct after the cover is jettisoned. The convex-shaped circular diverter separates flow into two sides. The last component is a streamlined body called a shell.

The operational envelope of subsonic airbreathing missiles is given in Figure 5. An operational plan serves as a reference point for determining optimization design conditions. It is assumed that a cruise missile featuring an inlet cover is carried by a UCAV which cruises at 10 km altitude

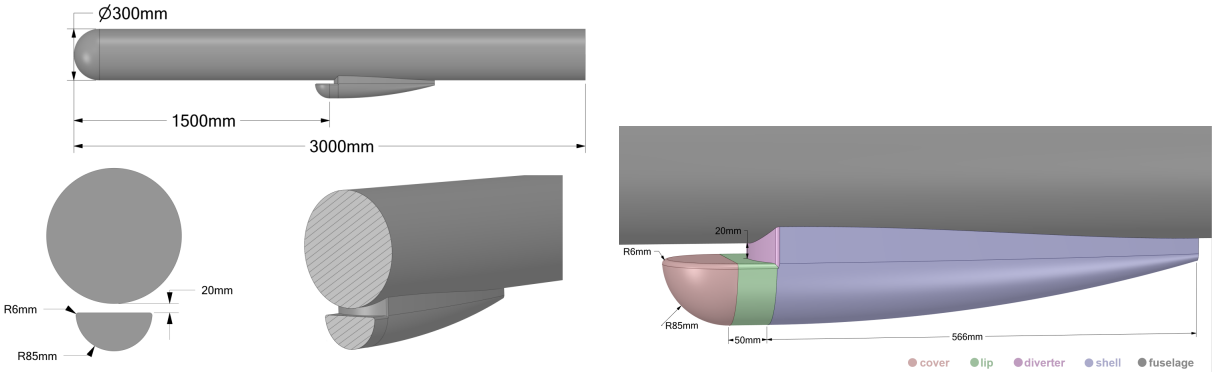

Figure 4: Baseline Configuration

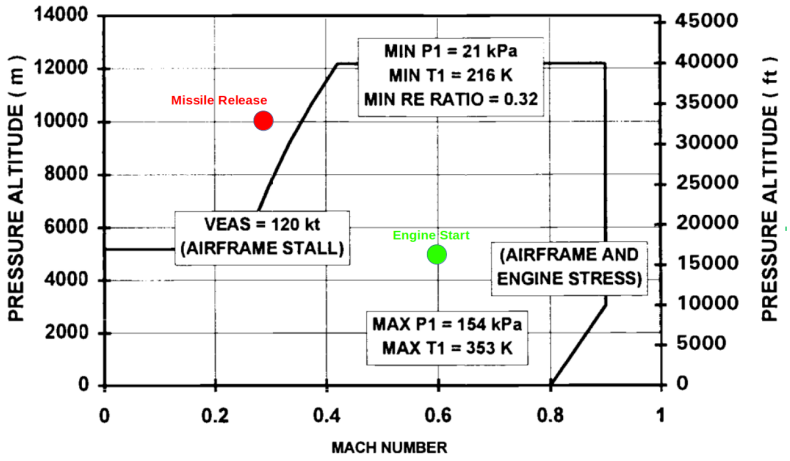

Figure 5: Operational Envelope of a Subsonic Airbreathing Missile [6]

and 0.3 Mach number. Inside the flight envelope of the missile, 5 km altitude and 0.6 Mach number are selected for the engine ignition and the cover ejection point.

3.2 Free Form Deformation Box and Geometric Constraints

In the optimization study, an FFD box is employed to represent and deform the engine inlet cover. The FFD box encapsulates the cover surface, as illustrated in Figure 6. The region inside the FFD box is defined as the design space. FFD boxes have lattice points along the cartesian coordinates. Since the movement of the lattice points deforms the surface encapsulated, the positions of the FFD box lattice points becomes the optimization variables. Each lattice point is associated with three variables due to its movement in three coordinate directions in space. The lattice points on the red planes are not allowed to move during the optimization process to keep the root section of the inlet cover fixed. In addition, the lattice points on the green planes are restricted to move within the plane to maintain a flat top surface. The remaining lattice points can move freely in three directions as long as they stay within the initial box. To investigate the effect of FFD box resolution in the optimization study, two FFD boxes with

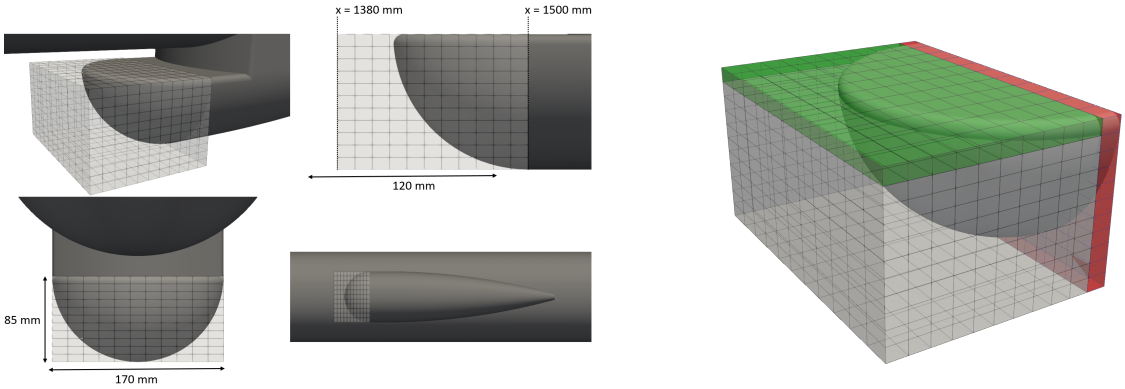

Figure 6: FFD Box

different numbers of lattice points are employed: One with a resolution of $9 \times 9 \times 9$ and the other one with a resolution of $12 \times 12 \times 12$.

3.3 Case I: Minimization of the Inlet Cover Drag

The drag minimization of the inlet cover is considered first. The objective function f is simply expressed as

$$f = C_{D_{\text{cover}}} \tag{2}$$

The optimization is performed for two FFD boxes, each with a different resolution, as given in Figure 7. The graph traces the evolution of the drag coefficient of the inlet cover throughout the optimization processes. Both optimization processes with the $9\times9\times9$ and $12\times12\times12$ FFD boxes converge toward the same optimum design conditions. Since the large number of design variables does not increase the cost of the gradient computations, the $12 \times 12 \times 12$ FFD box is chosen for conducting the optimization studies. Initially, a sharp decline in the drag coefficient of the cover is observed, succeeded by a gradual decrease until the value stabilizes around the 63^{th} step. The surface sensitivities in Figure 8 represent the change in the objective due to the perturbation of the surface nodes in the direction normal to the surface. Figure 9 shows the inlet cover shapes obtained during the optimization steps, progressively showcasing the design evolution from a quarter-sphere to a more streamlined form by elongating forward. Figure 10 shows the pressure distributions for the baseline and optimum designs. The baseline configuration displays a larger region with higher pressure values at the tip of the cover compared to the optimum design. The drag coefficient of the baseline cover is reduced from 0.0189 to 0.0142, which indicates an about 25% reduction.

3.4 Case II: Constrained Maximization of the Inlet Cover Opening Moment

Next, the maximization of the opening moment of the inlet cover with respect to the hinge axis is considered. The location of the hinge axis is shown in Figure 11. The drag coefficient of the overall configuration is also constrainted with an upper limit of 0.146, which is 10 percent higher than the baseline value. The objective function f and the constraint function g are

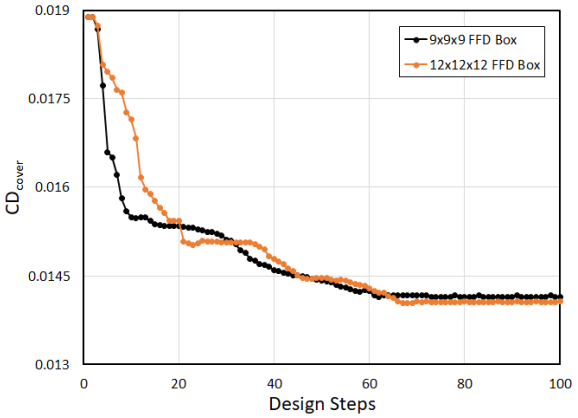

Figure 7: Variation of Drag on the Inlet Cover

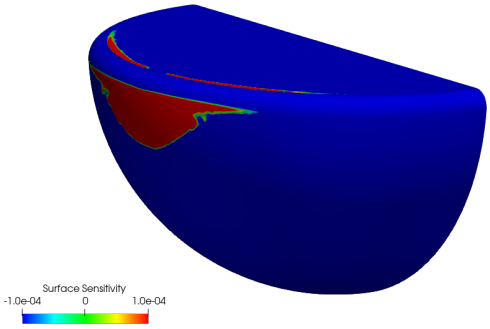

Figure 8: Initial Surface Sensitivity

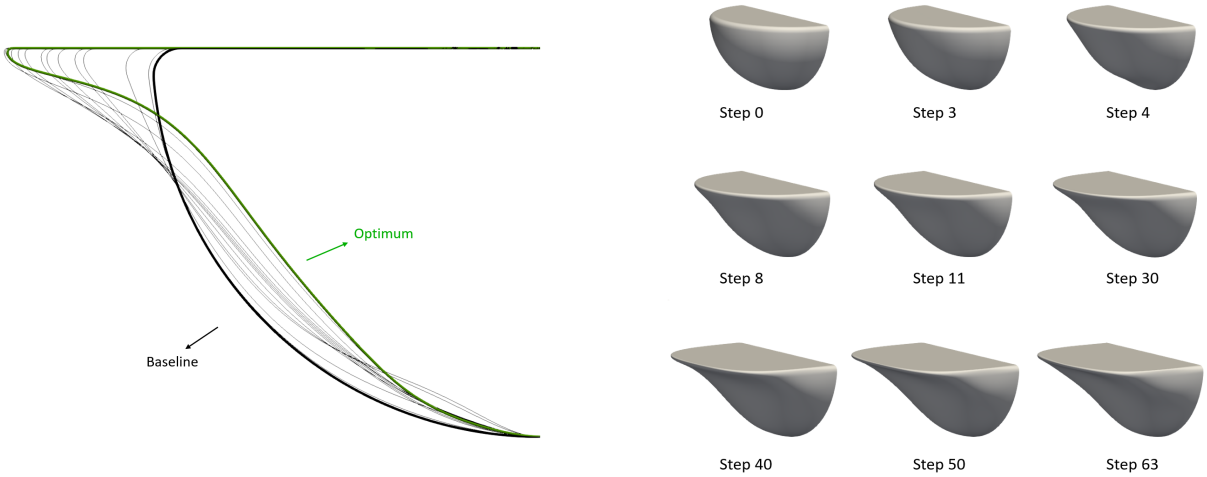

Figure 9: Inlet Cover Shapes along Optimization Steps

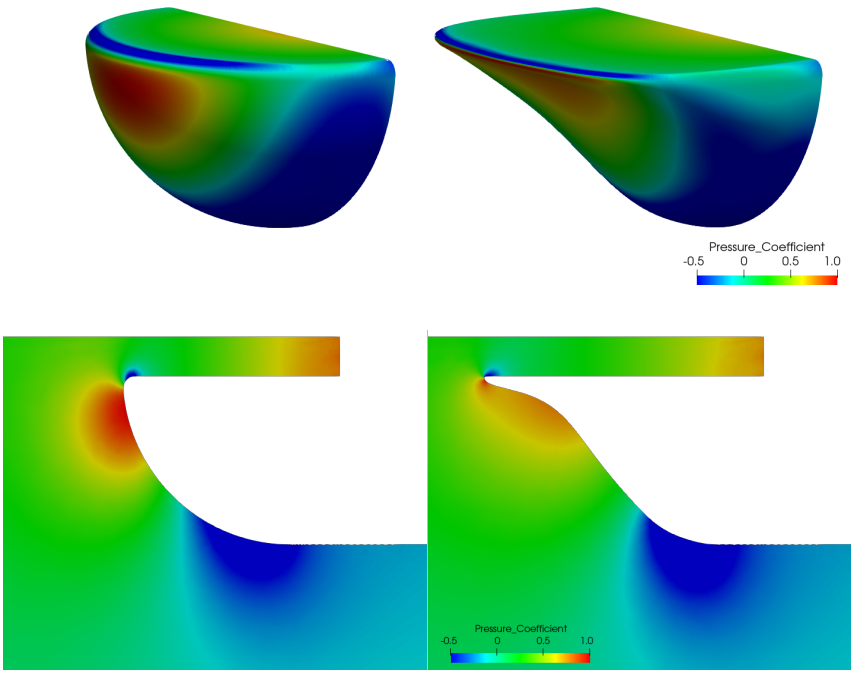

Figure 10: Pressure Distributions for Baseline (left) and Optimum (right) Configurations

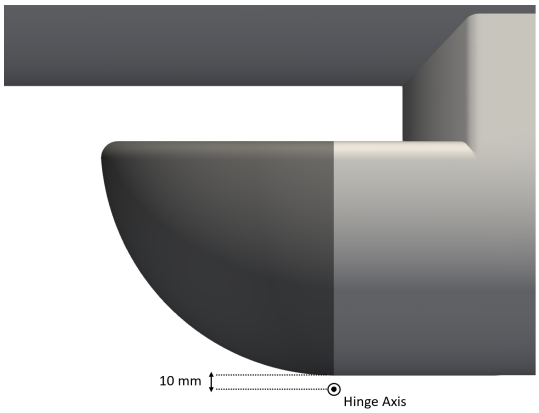

Figure 11: Inlet Cover Hinge Axis

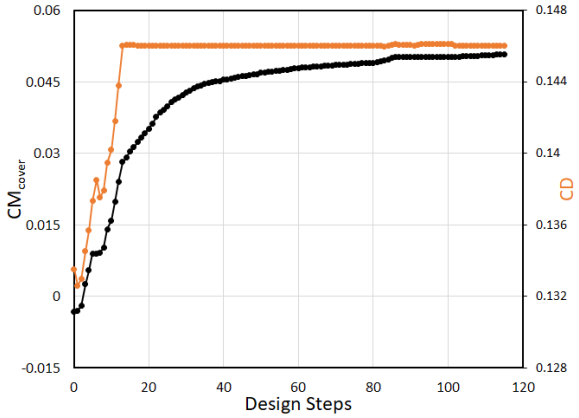

Figure 12: Variation of $C_{M_{\text{cover}}}$ and C_D along Optimization Steps

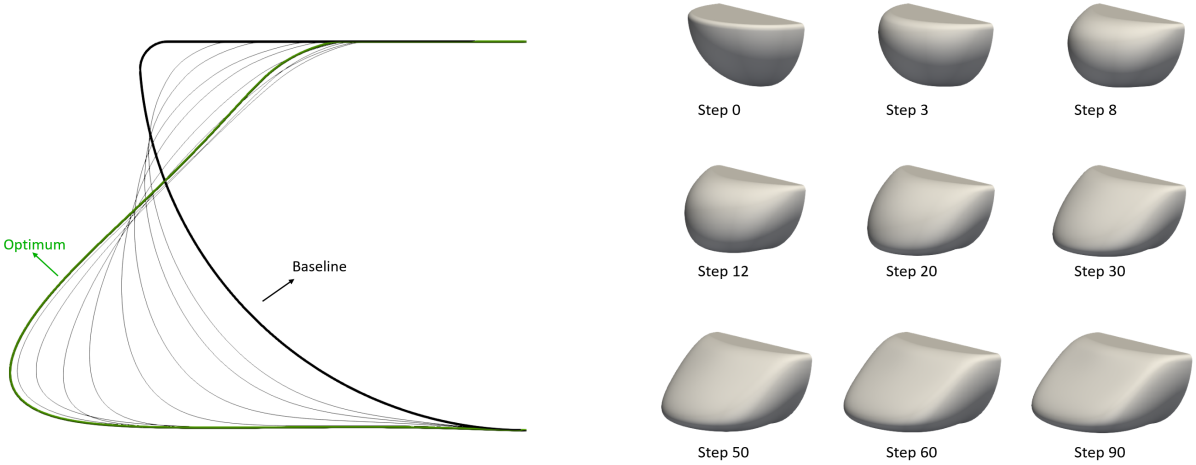

Figure 13: Inlet Cover Shapes along Optimization Steps

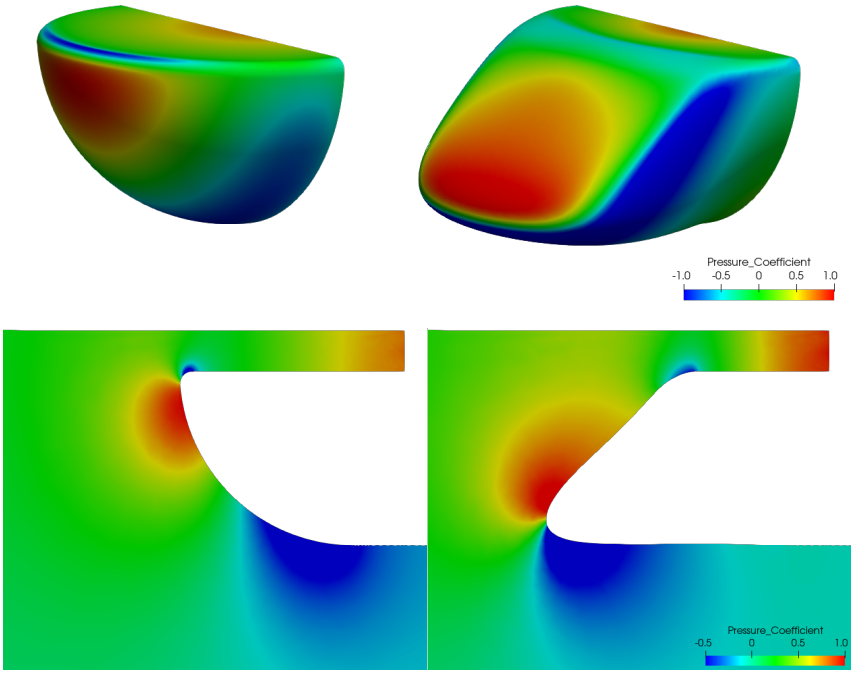

Figure 14: Pressure Distributions for Baseline (left) and Optimum (right) Configurations

expressed as

$$f = C_{M_{\text{cover}}} \tag{3}$$
$$g = C_D < 1.1 \times C_{D\,\text{baseline}} \tag{4}$$

Figure 12 shows the variation of $C_{M_{cover}}$ and C_D along the optimization steps. Initially, there is an abrupt increase in the $C_{M_{cover}}$ and C_D. By the optimization step 13, the drag coefficient of the overall configuration reaches 0.146, which serves as the upper limit of the drag constraint. However, $C_{M_{cover}}$ continues to rise gradually while C_D stays constant. The moment coefficient converges around the step 90. Eventually, the moment coefficient of the cover relative to the hinge axis increases from -0.0032 to 0.0399. The inlet cover shapes obtained during the optimization steps are illustrated in Figure 13. The gradual rounding of the shape up to design 8 is followed by a downward tapering and formation of an inclined plane on the front surface. The pressure distributions for the baseline and optimum designs are shown in Figure 14. As observed, the high-pressure area on the inclined plane now exerts an opening moment on the hinge axis rather than a closing one.

3.5 Case III: Multi-objective Optimization

In this case a multi-objective optimization is performed to reach an optimum balance between the conflicting objectives, namely, to minimize the drag due to the inlet cover while simultaneously increasing the opening moment with respect to the hinge axis. To implement this objective, a weighting factor is introduced into the objective function:

$$f(c) = C_{D_{\text{cover}}} - c \times C_{M_{cover}} \tag{5}$$

The factor c becomes a parameter. As it is increased, the importance of $C_{M_{cover}}$ is amplified. Figure 15 depicts a Pareto front, showcasing how changes in the weighting factor c impacts the relationship between $C_{D_{\text{cover}}}$ and $C_{M_{cover}}$. It offers an insight into how adjusting c influences the trade-off between drag reduction and pitching moment control in multi-objective optimization. As the value of c increases, both the drag and the opening moment of the inlet cover increase. As expected, the pareto front values fall between those of Case I and Case II. The pressure distributions corresponding to each value of c are illustrated in Figures 16. As c increases, the high-pressure region on the front surface enlarges, while a low-pressure region between the front and bottom surfaces becomes obvious. Additionally, the pressure distribution on the top flat surface remains relatively similar across different values of c. For $c = 0.1$, the drag is slightly higher than in Case I, yet the $C_{M_{\text{cover}}}$ increases. Moving to $c = 0.2$, the drag decreases compared to the baseline, and the $C_{M_{\text{cover}}}$ is around zero. At $c = 0.25$, there's a rise in drag compared to $c = 0.2$, but it comes with a positive opening moment. Progressing to $c = 0.3$, despite the drag being similar to the baseline, an increased opening moment is observed. Finally, the cases with $c = 0.4$ and $c = 0.5$ offer higher opening moments, with significantly lower drag compared to Case II.

4 CONCLUSIONS

In this study, an adjoint-based aerodynamic shape optimization of a missile engine inlet cover is successfully performed. The SU2 flow and adjoint solvers are utilized to minimize the

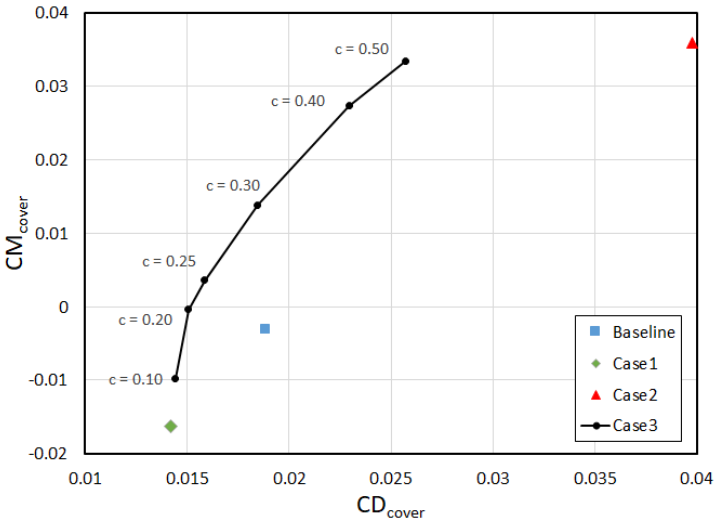

Figure 15: Pareto Front for Optimum Designs

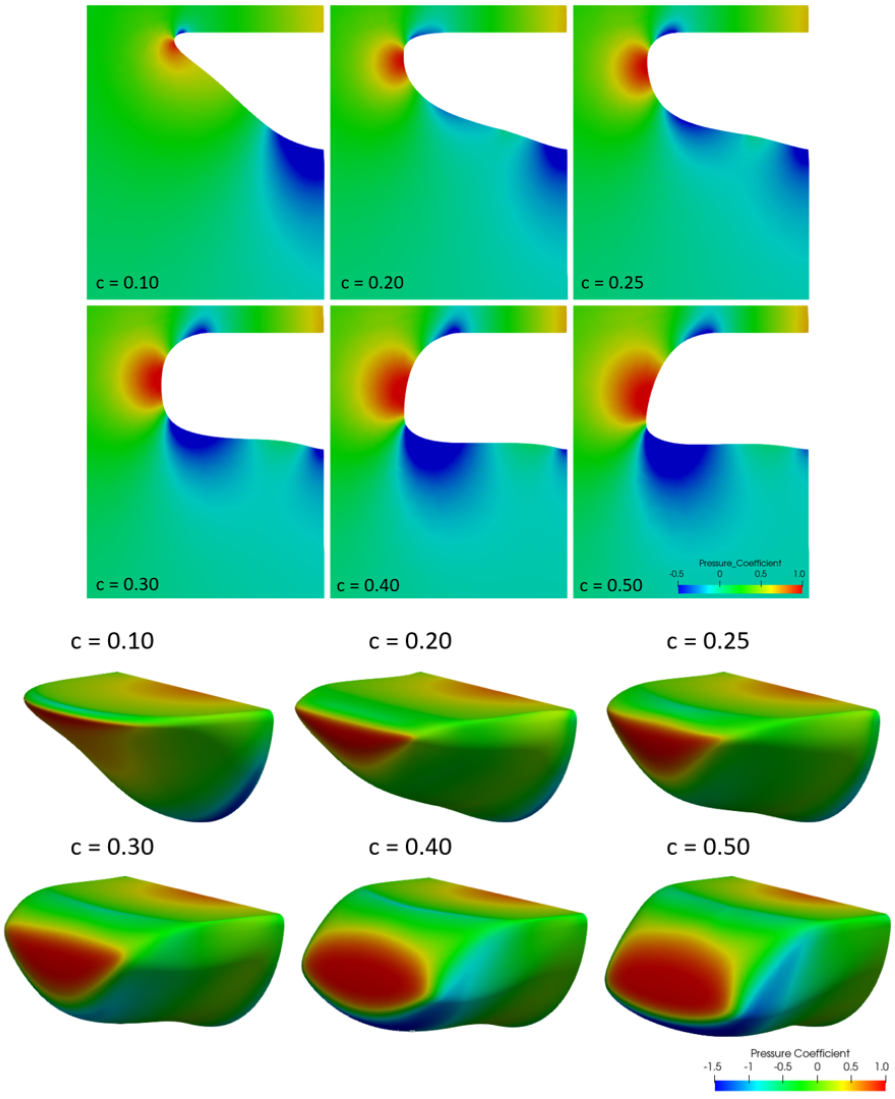

Figure 16: Pressure Distributions for Optimum Designs

drag and to maximize the opening moment of an engine inlet cover to enhance the capabilities of the missile system. The optimization studies focus on three distinct cases, each targeting different objectives. In the single-objective optimization to minimize the drag a 25% reduction is achieved. Whereas the maximization of the opening moment provides a self opening inlet cover. The multi-objective optimization produces a Pareto front of these competing objectives, which facilitates the discovery of optimum designs capable of simultaneously reducing drag and enhancing the opening moment. An optimum case provides the minimum opening moment with $C_{M_{\text{cover}}} = -0.0004$ while the drag induced is $C_{D_{\text{cover}}} = 0.0151$, which is still 20% less than the baseline drag.

The study shows that with CFD simulations and the adjoint-based shape optimization approach, significant improvements in the aerodynamic performance of an inlet cover are achieved, and an optimum design can be reached against the competing objectives. In addition, the present findings strongly indicate that the design of the missiles, where aerodynamic performance plays a critical role, can be significantly enhanced by adjoint-based shape optimization studies.

REFERENCES

[1] K. Parise, "Functional ground testing - evaluating the tomahawk cruise missile," in *30th Aerospace Sciences Meeting and Exhibit*, 1992.

[2] K. C. Giannakoglou and D. I. Papadimitriou, *Adjoint Methods for Shape Optimization*, pp. 79–108. Berlin, Heidelberg: Springer Berlin Heidelberg, 2008.

[3] S. P. Grossman and S. K. Laird, "Airstream ejected missile engine inlet cover," Aug. 26 1997. US Patent 5,660,357.

[4] P. Gomez, "Fado: Framework for aerostructural design optimization," 2020.

[5] J. Nagawkar, J. Ren, X. Du, L. Leifsson, and S. Koziel, "Single- and multipoint aerodynamic shape optimization using multifidelity models and manifold mapping," *Journal of Aircraft*, vol. 58, p. 591–608, May 2021.

[6] P. P. Walsh and P. Fletcher, *Gas turbine performance*. Blackwell Science, 2008.